analytical chemistry

pubs.acs.org/ac Article

Fast Diffusion Characterization by Multiphoton Excited Fluorescence Recovery while Photobleaching

Minghe Li, Aleksandr Razumtcev, Gwendylan A. Turner, Yechan Hwang, and Garth J. Simpson*

Cite This: *Anal. Chem.* 2023, 95, 14331−14340 Read Online

ACCESS | Metrics & More | Article Recommendations | Supporting Information

ABSTRACT: Multiphoton-excited fluorescence recovery while photobleaching (FRWP) is demonstrated as a method for quantitative measurements of rapid molecular diffusion over microsecond to millisecond timescales. Diffusion measurements are crucial in assessing molecular mobility in cell biology, materials science, and pharmacology. Optical and fluorescence microscopy techniques enable non-invasive rapid analysis of molecular diffusion but can be challenging for systems with diffusion coefficients exceeding ∼100 $\mu m^2/s$. As an example, fluorescence recovery after photobleaching (FRAP) operates on the implicit assumption of a comparatively fast photobleaching step prior to a relatively slow recovery and is not generally applicable for systems exhibiting substantial recovery during photobleaching. These challenges are exacerbated in multiphoton excitation by the lower excitation efficiency and competing effects from local heating. Herein, beam-scanning FRWP with patterned line-bleach illumination is introduced as a technique that addresses FRAP limitations and further extends its application range by measuring faster diffusion events. In FRWP, the recovery of fluorescence is continuously probed after each pass of a fast-scanning mirror, and the upper bound of measurable diffusion rates is, therefore, only limited by the mirror scanning frequency. A theoretical model describing transient fluctuations in fluorescence intensity arising as a result of combined contributions from photobleaching and localized photothermal effect is introduced along with a mathematical framework for quantifying fluorescence intensity temporal curves and recovering room-temperature diffusion coefficients. FRWP is then tested by characterization of normal diffusion of rhodamine-labeled bovine serum albumin, green fluorescence protein, and immunoglobulin G molecules in aqueous solutions of varying viscosity.

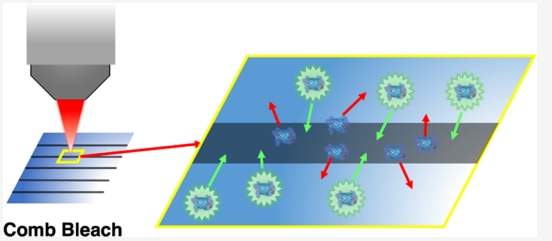

INTRODUCTION

Biochemical processes are frequently dictated by kinetics, such that quantitative characterization of molecular diffusion is critical to understanding physicochemical evolution in complex biological systems. Translational and rotational diffusion characteristics of macromolecules in biological media and within pharmaceutical formulations play a major role in regulating the rates of biochemical reactions and determining the bioavailability of therapeutics. Even though the mathematical framework for studying diffusion was derived by Fick almost two centuries ago, the introduction of precise and reliable methods to measure molecular diffusion greatly accelerated following the development of modern spectroscopic and microscopic techniques. Among the most commonly used translational diffusion characterization methods are dynamic light scattering (DLS), diffusion NMR (dNMR), single particle tracking, and fluorescence correlation spectroscopy (FCS).[1−6] In addition, fluorescence and phosphorescence anisotropy was carried out to characterize rotational motions of macromolecules in aqueous solutions.[7,8] Despite the demonstrated successes of these methods under appropriate conditions, the optical imaging methods for probing translational diffusion are generally limited to diffusion coefficient D values not exceeding 50 $\mu m^2/s$.[9] FCS and dNMR were shown to enable the characterization of faster diffusion, but the former is only applicable to highly diluted solutions, while the latter requires highly specialized instrumentation and is incompatible with solid samples.

Fluorescence recovery after photobleaching (FRAP) is another widely established method that enables diffusion characterization of biomolecules at micrometer scales.[10−12] In FRAP, a short exposure of a photobleaching laser irreversibly drives fluorophores in the focal volume into an inactive dark state. The following recovery of fluorescence intensity directly informs on the diffusion characteristics of fluorescent molecules spreading into the photobleached volume from the surroundings due to an established concentration gradient. FRAP has been widely utilized as a routine and reliable method to probe the mobility and chemical properties of fluorescently labeled biomolecules within cell organelles and membranes.[12−15] FRAP has also found applications in materials

Received: June 16, 2023
Accepted: August 30, 2023
Published: September 12, 2023

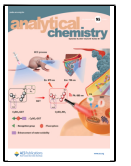

https://doi.org/10.1021/acs.analchem.3c02638
Anal. Chem. 2023, 95, 14331−14340

science for studying the diffusion of polymer chains and the mobility of dopants in glass materials.[16,17]

In the most common point-bleach implementation, FRAP is performed by bleaching a diffraction-limited single spot within a sample volume using a tightly focused high-intensity visible laser beam. However, the accuracy of recovered diffusion parameters in the point-bleach FRAP relies heavily on knowing the point-spread function (PSF) of the bleaching beam. Additionally, issues such as optical aberrations, misalignment, and optical turbidity can perturb the excitation beam focus, making it difficult to quantitatively estimate the bleach volume. Furthermore, in the conventional single-point bleach FRAP, local transient heating can negatively impact the measurement accuracy by altering the local diffusion properties and by thermally damaging the sample. Local heating is particularly problematic in multiphoton point-bleach FRAP experiments that require high peak laser fluences for efficient nonlinear excitation. However, it was demonstrated that careful selection of experimental parameters such as bleaching power enables accurate recovery of diffusion parameters with multiphoton-excited FRAP.[18]

None of the common diffusion characterization methods provide facile routes for mapping spatially varying diffusivities within structurally heterogeneous assemblies. Several previous studies have demonstrated the use of line and patterned illumination profiles to circumvent some of the limitations of conventional FRAP analysis.[19−21] Recently, Geiger et al. have demonstrated the theoretical framework and proof-of-concept experiments for Fourier-transform FRAP (FT-FRAP) with a comb-bleaching pattern across a large (∼1 × 1 mm) field of view (FoV).[22] Following the initial demonstration, FT-FRAP has recently been applied to characterize the mobility and chemical composition of phase-separated microdomains in amorphous pharmaceutical formulations.[23] In FT-FRAP, a periodic line bleach is achieved by controlling fast-scanning mirrors (either resonant or galvanometer scan mirrors) that rapidly translate the excitation beam across the FoV. In this implementation, a significant reduction in local heating is achieved by distributing the incident power along multiple equally separated rapidly scanned lines. Spatial frequency domain analysis results in sharp puncta in the spatial FT domain, by analogy with point-bleach in real space. Because of reduced local heating effects from rapid beam-scanning, comb-bleach FRAP is compatible with two-photon excited fluorescence (TPEF). The integration with TPEF is particularly advantageous in diffusion studies within structurally heterogeneous systems, leveraging the compatibility of TPEF with deep-tissue imaging through optically scattering media.

While FT-FRAP using periodically patterned illumination with analysis in the spatial FT domain circumvents many practical limitations of conventional FRAP, the time limit for fast-diffusing species is not fundamentally different from point-bleach methods. Just as in wide-field FRAP measurements, the upper bound of the studied diffusion coefficients in beam-scanning FT-FRAP is determined by the combination of the photobleach rate and the single frame acquisition time. Even assuming an instantaneous photobleach event, typical frame rates in high-sensitivity cameras of ∼60 fps result in a practical upper limit of diffusive motions on the order of $D < \sim 100$ $\mu m^2/s$. However, in practice, the photobleach process itself often dictates the upper bound on the diffusion rates directly accessible through FRAP (including FT-FRAP). Compared to fluorescence emission, photobleaching is a relatively rare event (1 in $\sim 10^6$ excitations), complicating the rapid generation of high bleach depths.[24] Substantial fluorescence recovery can potentially take place within the timescale of the photobleaching event for fast diffusion processes. Increasing the laser fluence in point-bleach measurements to shorten the photobleaching time can lead to saturation of the chromophores for optical-induced transparency and/or increases in the local heating rate raising the risk of permanent thermal sample damage. This latter point is particularly critical in multiphoton excitation given the high laser fluences typically used. FT-FRAP can mitigate both of these issues by distributing the photobleach power over the entire field of view, but still suffers from the fundamental speed limit associated with partial or complete recovery arising during the timescale of the photobleach step.

Further complicating the use of FRAP for fast diffusive motions, short-term reductions in fluorescence during rapid exposure to the excitation beam are expected not only from photobleaching itself but also from photothermal effects and other reversible photophysical interactions. In addition to irreversible reactions suppressing fluorescence, excited fluorophores can undergo reversible transitions (e.g., to long-lived triplet states), followed by recovery from photophysics rather than diffusion.[25,26] Furthermore, vibrational relaxation in the ground and excited electronic states together with nonradiative relaxation can produce local transient temperature increases. Given the high-temperature sensitivity of fluorescence quantum yields (∼1−2%/°C),[27] even transient temperature changes of only a few degrees could have a substantial impact on the fluorescence intensity, making it a particularly important consideration in quantitative multiphoton excited laser-based FRAP measurements.[28,29] The temperature sensitivity of fluorescent dyes is well-studied and was previously shown to be a highly accurate probe for biological processes dynamics, such as quantifying protein folding kinetics.[30,31] More recently, Simpson and Cheng's groups have independently demonstrated the use of thermosensitive fluorescent molecules for probing local mid-IR absorption through the quantification of the local photothermal effect.[32,33]

In the present work, the instrumentation and theoretical framework for fluorescence recovery while photobleaching (FRWP) analysis is introduced. FRWP is shown to support the quantitative analysis of fast (>50 $\mu m^2/s$) diffusion by monitoring the variations in fluorescence intensity during the photobleaching event. FRWP utilizes a high-speed resonance mirror for rapid beam-scanning that minimizes local heating effects and provides high temporal resolution. The local heating reduction enables the compatibility of FRWP with nonlinear two-photon excitation, opening the potential for high-fidelity imaging in turbid, heterogeneous media. The effect of residual local heating on the values of apparent diffusion coefficients was studied, quantified, and mathematically separated to ensure the recovery of the room-temperature diffusion coefficients for comparison with theoretical predictions. An empirically observed nonlinear dependence of the apparent diffusion coefficients on the incident laser power is discussed. FRWP analysis is applied to study the diffusion properties of natively fluorescent and externally labeled protein molecules in aqueous solutions that are usually incompatible with conventional FRAP due to their high mobility. The theoretical foundation of FRWP described herein using homogeneous samples provides a pathway for the further development of deep-tissue volumetric diffusion mapping

https://doi.org/10.1021/acs.analchem.3c02638
Anal. Chem. 2023, 95, 14331−14340

techniques, in which the diffusion coefficient varies as a function of 3D position within complex and heterogeneous biological assemblies.

EXPERIMENTAL METHODS

A custom nonlinear microscope system (Figure 1) was used for TPEF (800 nm excitation wavelength) FRWP analysis. The

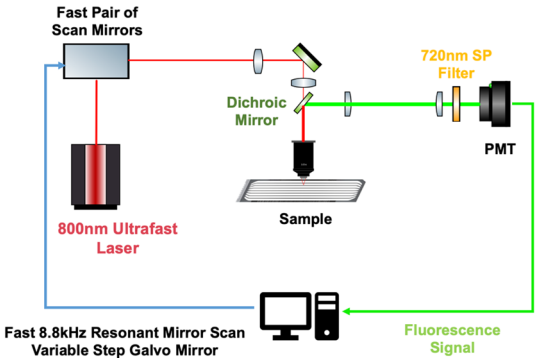

Figure 1. Simplified schematic depiction of the nonlinear optical beam-scanning microscope that was used for two-photon FRWP measurements. SP is a shortpass fluorescence filter; PMT is a photomultiplier tube.

excitation beam was produced by a tunable 80 MHz 150 fs Ti:sapphire ultrafast laser (Spectra Physics Mai Tai) with a maximum average output power of 1 W. The incident beam went through a galvo mirror (Cambridge Technologies) operating with a 16 Hz sawtooth motion for the slow-scan axis and an 8.8 kHz sinusoidal resonant mirror (Electro-Optical Products) for the fast-scan axis. Both mirrors were time-synchronized with a master clock set by the 80 MHz repetition rate of the laser. A Nikon 10×, 0.3 NA microscope objective was used to project the scan pattern onto the sample focal plane, and the TPE-UVF signal was collected in the epi direction through the same objective. The excitation power at the sample plane was around 100 mW over the whole field of view for two-photon excited photobleaching. The epi-detected fluorescence signal was filtered with a 720 nm shortpass fluorescence filter (Thorlabs FES0700) and directed to a Hamamatsu H10720 photomultiplier tube (PMT) module. The PMT response was digitized synchronously with the excitation laser pulses using a digital oscilloscope card (AlazarTech ATS9350) and reconstructed into 512 × 512 pixels images using in-house MATLAB algorithms, as described previously.[34] The image acquisition frame rate was 16 fps.

The FRWP experiment consisted of three consecutive stages, (1) pre-bleach imaging, (2) photobleaching, and (3) post-bleach imaging (Figure 2d), and is described in detail in the Theoretical Framework section. The pre-bleach images were generated using a standard 512-step square raster scan to reconstruct 512 × 512 pixels images. Comb patterns for patterned photobleaching were produced by modification of the analog control of the signal delivered to the position of the slow-scan galvanometer mirror. The protocol and software that enables the programming of custom galvo mirror scan patterns were described previously.[22] Rather than a smooth progression of the slow-scan voltage between upper and lower limits in 512 increments, the beam was directed in a stairstep pattern, with longer dwell times at discrete periodic locations within the field of view (Figure 2b,c). The two scanning approaches (full FoV raster scanning and periodic line bleaching) are illustrated in schematic animations (Movie S1). For a comb pattern with eight photobleach lines, the resonant mirror directed the beam across each for 64 consecutive passes before progressing to the next in the queue. The total number of fast-scan mirror periods per scan was maintained at 512, given by the product of the number of photobleaching stripes and the consecutive repeats per line per frame (e.g., 512 = 8 × 64).[34] Only the uniformly illuminated central section of each of the fluorescence images was used for the analysis, and the images were cropped prior to fitting.

Tetramethylrhodamine conjugated bovine serum albumin (BSA) was purchased from Thermo Fisher Scientific. A series of glycerol and phosphate-buffered saline (PBS) (pH 7.4) solutions were mixed at room temperature. The glycerol volume percentage ranged from 0 to 40%. BSA solutions were made by dissolving 2 mg of BSA lyophilized powder in 1 mL of mixture buffer solution. Green fluorescent protein (GFP) expressed in *E. coli* was purchased from Sigma-Aldrich. GFP was originally stored in PBS containing 20% glycerol. Rhodamine-labeled goat anti-mouse immunoglobulin G (IgG) secondary antibody was purchased from Thermo Fisher Scientific and solubilized in PBS. Solutions were mixed thoroughly before FRWP analysis. The buffer solutions were made from thorough mixing of glycerol with PBS solution to tune the viscosity.[30]

Theoretical Framework. *Fluorescence Recovery during the FRWP Measurements.* The complete mathematical description of fluorescence intensity trends during the photobleaching process requires considering the decrease in the concentration of active fluorophores being photobleached (the downward part of each of the experimental "teeth") and the diffusion-dictated recovery driven by the resulting concentration gradient. For uncorrelated photobleaching probabilities with nominally identical fluorophores, the photobleaching trend at a constant excitation power is described by an exponential decay:

$$C(x, t)_{i+1} = C_0(x, t)_i[1 - (1 - e^{-\alpha t})e^{-x^2/2\cdot\sigma_b^2}] \quad (1)$$

In eq 1, $C(x,t)$ is the concentration of unbleached fluorophores at time t and position x, C_0 is the initial concentration, σ_b is the root mean square width of the bleaching laser, and α is the photobleaching rate. The equation consists of two exponential relationships, which describe the temporal and spatial fluorophore concentration changes. The $e^{-\alpha t}$ derives from the integral of a fixed percentage photobleaching efficiency each single-pass of the fast-scan mirror. The term $e^{-x^2/2\cdot\sigma_b^2}$ represents the Gaussian PSF of the Gaussian photobleach spot. A Taylor-series expansion about time zero gives the following expression for the exponential function of the time-dependent recovery. For short timescales, only the leading term in the expansion was considered significant:

$$C(x, t)_{i+1} = C(x, t)_i\left[1 - \left(\frac{(\alpha t)}{1!} - \frac{(\alpha t)^2}{2!} + \frac{(\alpha t)^3}{3!} - \ldots\right)\cdot e^{-x^2/2\cdot\sigma_b^2}\right]$$

$$\cong C_0(1 - \alpha t\cdot e^{-x^2/2\cdot\sigma_b^2}) \quad (2)$$

https://doi.org/10.1021/acs.analchem.3c02638
Anal. Chem. 2023, 95, 14331−14340

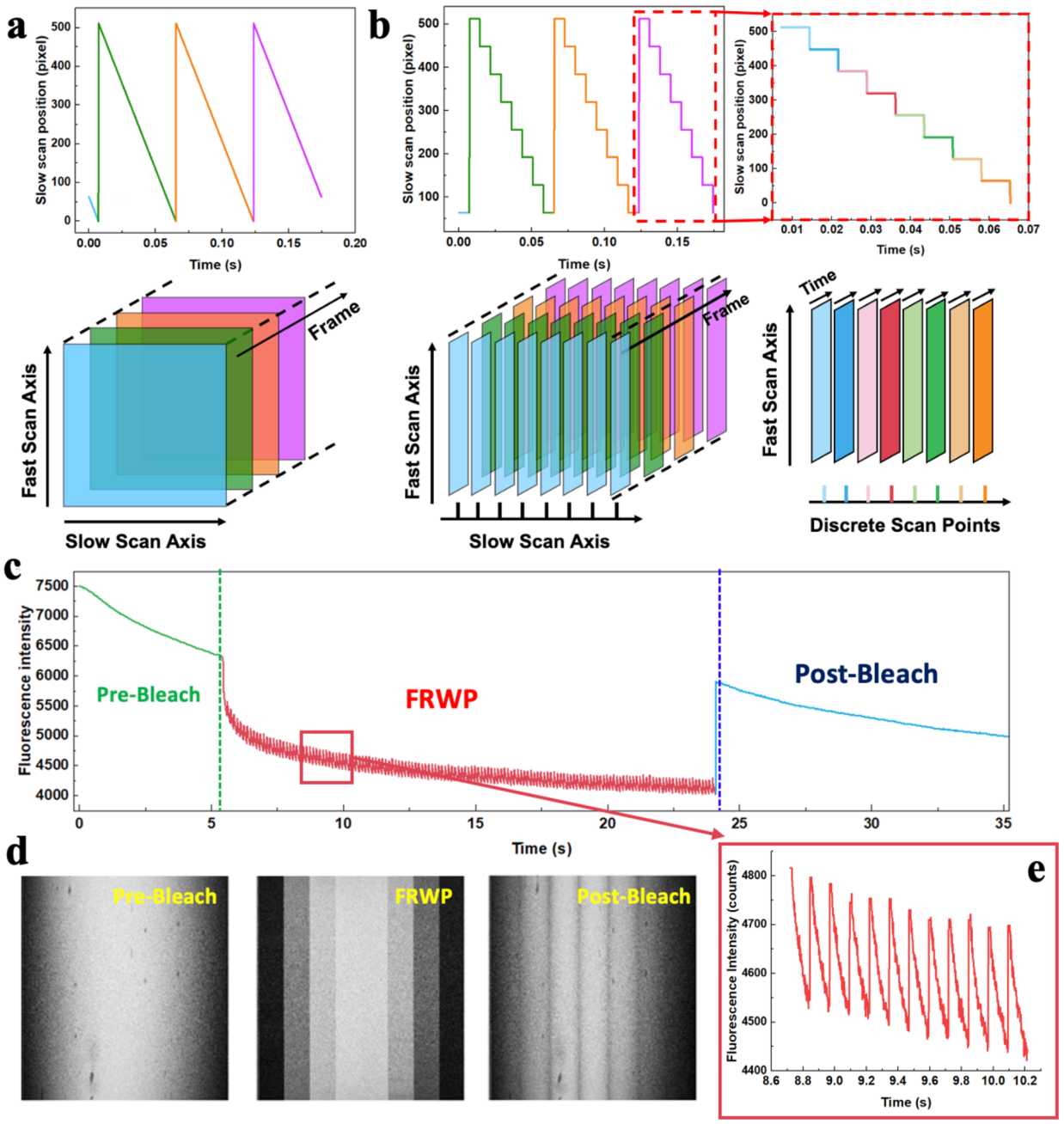

Figure 2. Overview of the FRWP analysis pipeline. (a) Galvo scan mirror position time trace during a full FoV raster scanning in the pre- and post-bleach stages. (b) Galvo position time trace during an eight-line step scan in the FRWP stage. (c) Example of a full raw data trace over all three stages of the FRWP process. (d) Representative images of a fluorescence FoV at each stage of the analysis. Only 8 selected lines are scanned during the FRWP stage with 64 passes over each line to match a total of 512 scan lines. Residual bleached lines can be seen during a full FoV imaging in the post-bleach stage. (e) Zoom-in showing the experimental sawtooth pattern in detail.

Using the approximation in eq 2, the initial pre-bleaching decay can be expressed as a linear concentration reduction proportional to the photobleaching rate at a certain position, agreeing well with the pre-bleach stage observations in Figure 2.

Once the concentration gradient of active fluorophores is established by an excitation laser, molecular diffusion takes place. Normal molecular diffusion is described by Fick's second law of diffusion, relating the time derivative of the concentration to its gradient. In FRAP experiments, irreversible photobleaching within the illuminated locations induces a concentration gradient of active fluorophores from the surroundings. The diffusion tensor D describes the spatial variance of the molecular mobility in a 3D space:

$$\frac{\partial C(r, t)}{\partial t} = \nabla \cdot [D \nabla C(r, t)] \tag{3}$$

where C is the concentration distribution of the fluorophore, D is the diffusion coefficient tensor, and t is the time.

Notably for the comb-patterned photobleaching (illustrated in Figure 2b) in an initially isotropic medium, the diffusion tensor can be replaced by a scalar D and the concentration distribution is a simple function C of the distribution in concentration along a single dimension, x, orthogonal to the

https://doi.org/10.1021/acs.analchem.3c02638
Anal. Chem. 2023, 95, 14331−14340

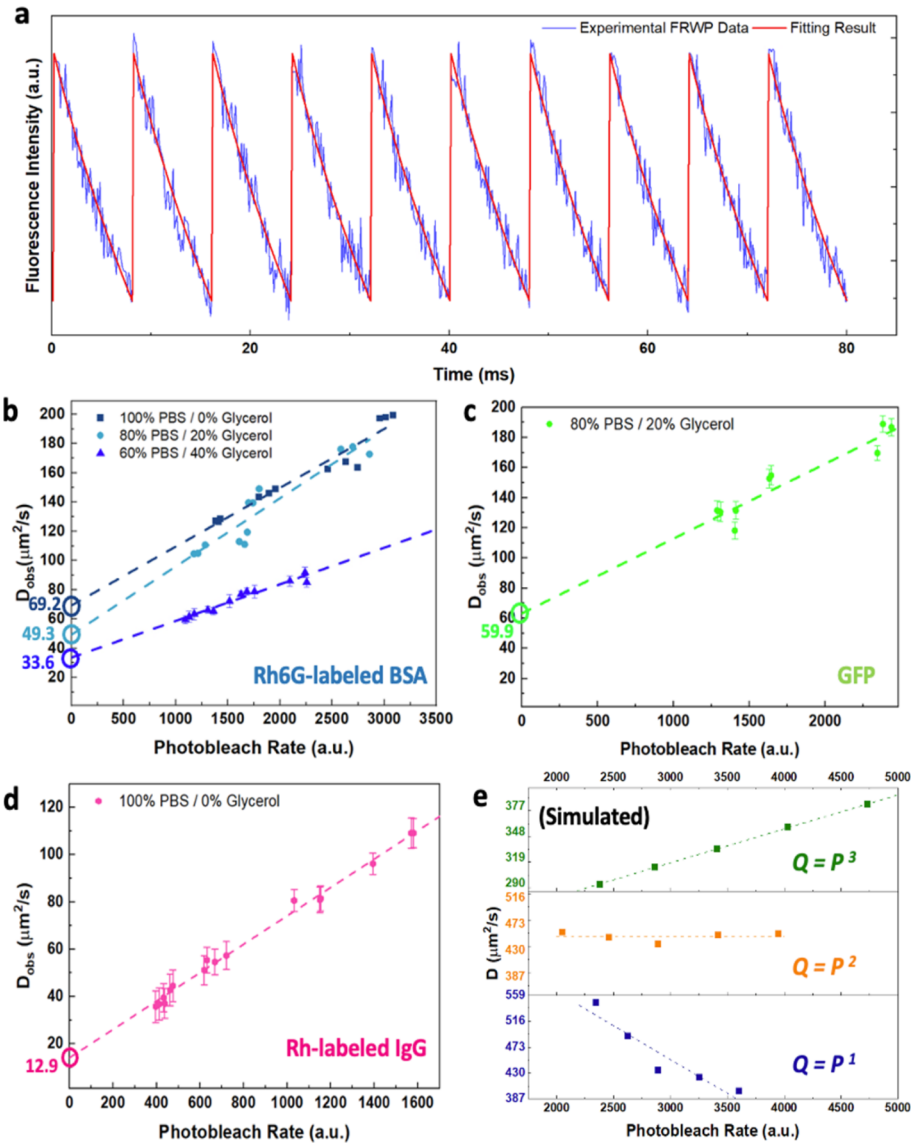

Figure 3. (a) Representative example of a FRWP fitting result. (b–d) Measured apparent diffusion coefficients of aqueous solutions of various macromolecules (a) Rhodamine-labeled BSA, (b) GFP, and (c) Rh-labeled IgG) as the function of the photobleaching rate (proportional to the square of the incident laser power). The *y*-intercept values correspond to room-temperature diffusion coefficients in the absence of laser-induced photothermal effect and thermal diffusion. The error bars for two intersecting lines in b are omitted for visual clarity. (e) Validation of the linear fitting for diffusion coefficients using molecular and thermal diffusion forward model. The simulated plots demonstrate the dependence of the apparent D values on the order of the "deposited heat–laser power" relationship. The plots suggest a highly nonlinear relationship between the Q and P with a higher than quadratic dependence.

comb lines (diffusion parallel to the bleached lines and out-of-plane diffusion along the z-axis are considered negligible for thin samples):

$$\frac{\partial C(x,t)}{\partial t} = D\frac{\partial^2 C(x,t)}{\partial x^2} \tag{4}$$

Numerical solutions to eqs 2 and 4 based on the Euler method were evaluated in MATLAB in a "forward model", designed to replicate the FRWP observables for a set of given input parameters. Per the consideration above, the simulation included two phases: (i) the photobleaching phase, corresponding to repeated illumination of a single "tooth" in the comb (see results and discussion) and (ii) the recovery phase, during which the beam is occupied in the illumination of the other teeth in the comb. Recovery was assumed to arise orthogonal to the tooth direction, assuming a Gaussian PSF consistent with the use of an excitation beam underfilling the back pupil of the objective. For every simulation time step, the concentration profile in x was updated based on eqs 2 and 4. For a comb-bleach with eight teeth, the photobleaching happens within one-eighth of the frame time, with the pixel dwell time τ calculated as

$$\tau = \text{frame\_time}/(\#\text{pixel} \times \#\text{line}) \tag{5}$$

Given that the frame rate, the number of teeth in the comb, and the beam profile are known, the only variables in the forward model are the photobleaching rate α and the diffusion coefficient D. The former α can be determined directly from the baseline fluorescence reduction during the pre-bleaching stage. Initial guess values for D were predicted by the Stokes–Einstein diffusion equation and were used to initiate

https://doi.org/10.1021/acs.analchem.3c02638
Anal. Chem. 2023, 95, 14331−14340

Table 1. Comparison of Stokes−Einstein Estimation and FRWP Results for BSA in Various Viscosity Media

	100% PBS/0% Glycerol BSA	80% PBS/20% Glycerol BSA	60% PBS/40% Glycerol BSA	80% PBS/20% Glycerol GFP	100% PBS/0% Glycerol IgG
dynamic viscosity, Pa*s	8.93×10^{-4}	1.73×10^{-3}	4.05×10^{-3}	1.73×10^{-3}	8.93×10^{-4}
hydrodynamic radius, nm	3.48[37]			2.21[38]	6.5−13[39,40]
Stokes−Einstein prediction, $\mu m^2/s$	71.9	37.1	15.9	57.1	18.6−37.3
FRWP experimental value, $\mu m^2/s$	69.2 ± 7.7	49.3 ± 10.3	33.6 ± 2.8	59.9 ± 14.6	12.9 ± 1.6

Levenberg−Marquardt nonlinear curve fits to recover the maximum likelihood estimate values for D (Figure 3a). Prior to fitting to recover D, the sawtooth data were high-pass filtered to remove the rolling background. The recovered values of D were highly covariant with the measured value of the PSF width of the excitation beam, which was presumed to be a 2D Gaussian function of root mean square width σ_b. Accurate determination of σ_b was performed by image analysis following comb-bleach illumination of a rhodamine 6G dye cast within a high-viscosity nitrocellulose matrix (nail polish) to ensure negligible translational diffusion. Under these conditions, Gaussian fits of the stripe widths were used to recover values for σ_b.

High-Level Overview of the FRWP Approach. A timing diagram illustrating the data collection pipeline is shown in Figure 2. Prior to patterned photobleaching, the excitation source was scanned across the entire field of view in a raster pattern used for conventional beam-scanning imaging (pre-bleach stage, Figure 2a). Frame-to-frame reduction in fluorescence observed as a negative slope of the intensity trend in the "pre-bleach" stage in Figure 2c was used to establish the baseline photobleaching rate over the whole FoV. For the next step (patterned photobleaching), the raster pattern was changed to a "stair-step" pattern with longer dwell times at a select number of periodically spaced lines within the FoV, as shown in Figure 2b. Within a given line, the fluorescence was reduced following repeated sequential passes in a given "stair", followed by partial recovery at that location, as the beam was moved elsewhere to illuminate other "stairs". By nature of the periodicity in the pattern, the recovery time is identical between each sequential pass across a given "stair", allowing the entire data set to be pooled (Figure 2b). Finally, the beam is switched back to a full raster scan to once again perform full FoV imaging (post-bleach stage). For molecules with sufficiently slow diffusivity, residual photobleached lines persist (Figure 2d), enabling conventional FRAP analysis. However, the analysis of fluorescence changes occurring during the photobleaching process provides complimentary access to diffusion events happening at faster timescales.

A full raw experimental fluorescence intensity time trace for a single FRWP measurement is shown in Figure 2c with the three experiment stages clearly distinguishable. A gradual decrease in the overall fluorescence due to slow photobleaching during the full FoV illumination can be observed during stages (1) and (3), while the comb-bleaching FRWP analysis stage is characterized by a repetitive cycle of rapid bleaching and recovery creating a sawtooth pattern. The zoom-in of the sawtooth pattern is shown in Figure 2e. It should be noted that fluorescence recovery in stage (2) happens while the probe beam is bleaching other lines in the FoV, which creates an apparent sudden recovery in the upward part of each of the "teeth".

RESULTS AND DISCUSSION

The performance of FRWP analysis was first evaluated on solutions of rhodamine-labeled BSA in glycerol/PBS mixtures. BSA plays many biological roles in stabilizing oncotic pressure within capillaries, transporting fatty acids, bilirubin, minerals, and hormones, and functioning as both an anticoagulant and an antioxidant.[35,36] A concentration series of solutions containing increasing amounts of glycerol (from pure PBS up to 40% of glycerol) was studied to investigate the dependence of recovered apparent diffusion coefficients on the viscosity of the solutions. Furthermore, the experiments were performed at varying incident laser powers to isolate the contributions of thermal diffusion and photothermal effect.

In general agreement with expectations for processes driven by two-photon absorption, plots of the apparent diffusion coefficient (Figure 3b) for rhodamine-labeled BSA yield recovered values of D that scale quadratically with incident laser power and linearly with the excitation/photobleach rates. The values of photobleach rates at each power setting were determined from the "pre-bleach" stage fluorescence loss rate recorded over the entire field of view (Figure 2a,c) and scaled quadratically with incident laser power, consistent with expectations for two-photon excitation. From the intensity-dependent apparent diffusion coefficient, the molecular diffusion coefficient can be isolated by extrapolation to the intercept, corresponding to the observed diffusion coefficient in the limit of zero incident laser power. In this extrapolated limit, both the power-dependent contributions from thermal diffusivity and/or excited state recovery contribute negligibly. Based on simulations shown in Figure 3e, the slope of the curves depends on the intensity-dependent nonlinear scaling of the local heating, which in turn depends sensitively on measurement conditions (e.g., tightness of focus, optical aberrations, pulse duration, etc.). The non-monotonic dependence of the slope with glycerol concentration shown in Figure 3b is tentatively attributed to subtle changes in the tightness of focus, given that the 20% glycerol data were acquired on a different day than the other data on the curve. Nevertheless, the simulations suggest negligible dependence of the intercept on the scaling coefficient that dictates the slope. Each data point in Figure 3 represents a single time-dependent fit to recover the diffusion coefficient performed at a fixed incident excitation power, with representative uncertainties given by the 95% confidence intervals in the recovered parameters from the fits.

The validity of this extrapolation approach can be evaluated by comparison of the asymptotic translational diffusion coefficients with expectations for normal diffusion based on the Stokes−Einstein diffusion coefficient. The BSA diffusion coefficient can be estimated from the first principles by eq 6 for spheroidal particles in liquids with low Reynolds numbers.[33,34]

https://doi.org/10.1021/acs.analchem.3c02638
Anal. Chem. 2023, 95, 14331−14340

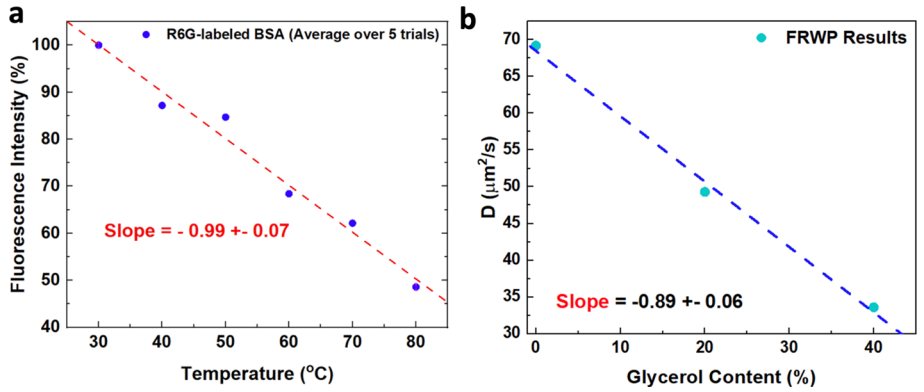

Figure 4. (a) Temperature dependence of the fluorescence intensity of Rh-labeled BSA measured a heat stage. (b) Dependence of FRWP-measured steady-state diffusion coefficients on the glycerol concentration in studied solutions.

$$D = \frac{k_B T}{6\pi\eta R} \tag{6}$$

In eq 6, k_B is the Boltzmann constant, T is the absolute temperature, η is the dynamic viscosity, and R is the hydrodynamic radius of the spherical particle. The hydrodynamic radius of the BSA can be measured by multichannel DLS, and the value used for the Stokes−Einstein equation was 3.48 nm.[37] The predictions from the Stokes−Einstein equation summarized in Table 1 are in good agreement with the experimentally recovered translational diffusion coefficients given by the intercepts of the curves shown in Figure 3.

Building on the proof-of-concept measurements with BSA, TPEF FRWP measurements were performed to quantify the molecular diffusivity of a small intrinsically fluorescent protein (GFP). GFP, first isolated from *Aequorea Victoria* jellyfish, is widely used as a biomarker for biological systems due to its compatibility with genetic tagging for exogenously expressed proteins, together with its brightness and high photostability. Translational and rotational diffusion of GFP in solution and cell cytoplasm have been previously thoroughly characterized by conventional FRAP and fluorescence anisotropy. However, due to its small radius and relatively fast diffusion, previous GFP studies were mostly conducted in highly viscous media (>60% glycerol content).[41,42] The room-temperature GFP diffusion coefficient in a 20/80 glycerol/PBS solution was measured by FRWP to be 59.9 $\mu m^2/s$, as shown in Figure 3c. Additional "book-end" studies were performed to interrogate molecular diffusion of a relatively large protein (immunoglobulin G, or IgG) with multiphoton excitation. IgG antibodies are the most common type (~80%) of antibody found in blood circulation, where they exist at levels (~70 μM) second only to albumin (500−800 μM).[43,44] The IgG diffusion is critical in modulating the human immune system and serves as a model surrogate for antibody-drug conjugates. The lyophilized IgG was dissolved in a PBS buffer solution. From the intercept in the data shown in Figure 3d, the recovered diffusion coefficient was 12.8 $\mu m^2/s$, consistent with its larger hydrodynamic radius (13−6.5 nm) relative to BSA (3.48 nm) and GFP (2.21 nm).[38,45,46] The authors were unable to find previously published data on the hydrodynamic radius of the particular goat IgG antibody that was used in the present work; however, the FRWP results might indicate that it was on the larger side of the cited range.

While the general trends between experimental and Stokes−Einstein predicted diffusion coefficients are in good agreement, the Stokes−Einstein prediction appears to underestimate the observed diffusion coefficients measured at high glycerol concentrations. Several sources of bias under these conditions were considered. The ability to perform FRWP measurements with low sample volumes (~10 μL), while advantageous, also has the potential to introduce high relative uncertainties in concentrations from subtle differences in volumes dispensed from micropipettes. The higher viscosity of glycerol solutions could exacerbate volumetric uncertainties and potentially introduce bias to overestimate the anticipated volume of viscous media delivered for pipettes calibrated for aqueous media. Additional sources of bias may potentially arise from incomplete mixing with highly viscous glycerol solutions, potentially resulting in inhomogeneous locations of higher or lower viscosity within the sampled volumes.

To test the potential importance of incomplete mixing, studies were undertaken to quantify the glycerol-dependent diffusion coefficient, recovered by the intercept in the limit of low laser excitation power. As illustrated in Figure 3, the results of the glycerol-dependent diffusion for rhodamine-labeled BSA are shown in Figure 4b. In brief, the results demonstrate a clear linear trend of decreasing diffusion coefficient with increasing glycerol concentration. This linear trend is consistent with expectations from the Stokes−Einstein formula in eq 6 in the limit of small changes in viscosity. Based on these results, it is reasonable to conclude that the sample preparation protocols adopted produced droplets that were well-mixed. Therefore, the small but statistically significant bias in diffusion coefficients stated in Table 1 are attributed to inaccuracies in the high-viscosity volumes dispensed by micropipetting.

Given the substantial perturbation in the apparent diffusion coefficient arising from local heating evident in Figure 3b−d, it is worth considering in more detail the role of transient local heating in multiphoton excited FRAP and FRWP. If the nonzero slopes observed in Figure 3 are attributed exclusively to local heating, an upper bound on the local temperature change can be calculated from the relative change in fluorescence. Temperature dependence of fluorescence intensity for the rhodamine-conjugated BSA solution used in this work was studied by monitoring the average fluorescence intensity of a calibration sample on a heating stage in the 30−80 °C temperature range. The average fluorescence signal was decreasing by 0.99 ± 0.07%/°C (Figure 4a). From the representative raw data shown in Figure 2e, an average change of ~5% was observed in the fluorescence during repeated sequential passes of the fast-scan mirror, corresponding to

https://doi.org/10.1021/acs.analchem.3c02638
Anal. Chem. 2023, 95, 14331−14340

temperature changes of ~5 °C. One might expect this increase in temperature to affect the molecular diffusivity, as temperature appears in the numerator in eq 6. However, a temperature change of 6 °C is only expected to produce a change in molecular diffusivity of ~2% according to the Stokes−Einstein equation, which is much less than the degree of perturbations observed in Figure 3. Furthermore, thermal diffusivity is much faster than molecular diffusivity, with a thermal diffusion coefficient of 143,000 $\mu m^2/s$ in water.[47] Rapid equilibration with the bath is expected during the quiescent unsampled recovery periods indicated in Figure 2 by the vertical rise in the sawtooth time traces. As such, the transient increase in temperature is expected to produce a negligible impact on the molecular diffusion coefficient under the conditions in which these measurements were made.

However, temperature changes upon transient local heating can also impact the fluorescence intensity directly through the photothermal effect, in which the quantum efficiency of fluorescence is reduced as the temperature is increased. Thermally induced suppression of fluorescence through the photothermal effect would manifest qualitatively similarly to FRAP but recover with the timescale of thermal diffusivity rather than molecular diffusivity. Least-squares fitting to a recovery arising from the combined effects of these two concurrent recovery mechanisms with different kinetics to a single diffusion coefficient will generally produce an outcome given by the weighted combination of the two diffusion coefficients. The relative amplitude of each process will generally vary with incident intensity according to their respective intensity dependencies. For two-photon excitation, FRAP will scale quadratically with the incident intensity. Depending on the intensity dependence of transient local heating, the scaling could range from linear if dominated by one-photon absorption through highly nonlinear from cascaded excited state absorption. The following general form of the relationship between the deposited heat (Q) and the incident laser power (P) was used with x being an adjustable exponent.

$$Q \propto P^x \tag{7}$$

In order to evaluate the FRWP trends in the presence of non-negligible intensity-dependent local heating, simulations were performed in which the exponent of the fluorescence excitation and heating was varied. The measured fluorescence photobleaching rate α was assumed to scale quadratically with excitation power, with power scaling between linear and cubic considered for local heating. A series of simulation results were generated using an updated forward model considering both molecular and thermal diffusion contributions and assuming a fixed molecular diffusion coefficient of 200 $\mu m^2/s$ at varying laser power. The simulation results were then fitted using a Levenberg−Marquardt nonlinear algorithm to recover the observed values D_{obs}. The fitting results are shown in Figure 3e. The trends are in excellent agreement with simple intuition; heating scaling with an exponent lower than 2 will become less important than two-photon excitation with higher peak laser power, while scaling greater than 2 suggests an increasingly important perturbation from local heating with higher power.

As can be seen from the simulation results, a positive slope of the observed diffusion coefficient D_{obs} suggests a higher than quadratic dependence of the local heating on incident laser power in the experiments. The observation of local heating effects scaling higher than quadratically is consistent with prior reports in multiphoton microscopy. Multiple previous studies focused on quantifying the dependence of photodamage on incident laser power in two-photon fluorescence microscopy reported high nonlinearity with scaling factors ranging from 2.14 to 3.17.[48−50] Consistent with these studies, the observed temperature change is attributed to a combination of one- and two-photon absorption together with additional nonlinearity attributed to cascaded absorption from excited vibrational/electronic states. In this limit, the simulations demonstrate reliable recovery of the molecular diffusion coefficient from the intercept of D_{obs} in the asymptotic limit of low laser power. Consistent with these simulated results, molecular diffusion coefficients evaluated from the intercept yielded values in good agreement with simple Stokes−Einstein estimations based on hydrodynamic radii.

Given the prominent role of local heating in the measured diffusivity in FRWP, a series of simulations were performed to assess the limiting behaviors expected in FRWP experiments in Figure 5. In brief, the figure shows two sequential processes

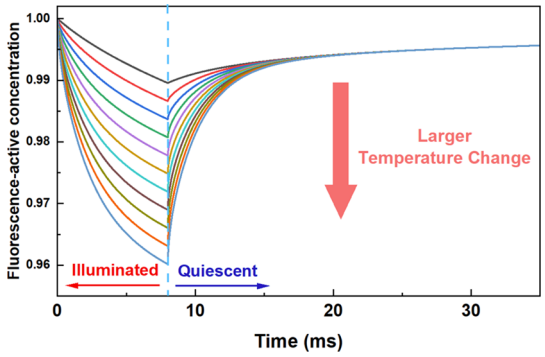

Figure 5. Simulations of temperature-dependent effects on FRWP during molecular diffusion analysis.

critical to FRWP recovery: (i) the illumination period on a single line and (ii) the quiescent period during illumination of other lines in the field of view. During the illumination period, reductions in fluorescence are modeled to arise from a combination of both photobleaching and local heating through the photothermal effect. Following cessation of illumination, high thermal diffusivity results in rapid recovery back to baseline over timeframes much faster than the quiescent period. As such, the effectively complete baseline recovery in temperature prevents direct measurement of the rate of recovery from the accessible FRWP measurements. It also suggests that any local transient temperature changes during illumination are rapidly dissipated and unlikely to significantly affect the much slower molecular diffusivity of key interest in this study.

While the primary focus of the present study is on FRWP with multiphoton excitation for high-accuracy diffusion analysis of rapidly diffusing species, the fortuitous direct access to local temperature changes from photothermal effects may provide a convenient approach for quantifying propensities to thermal damage in broad classes of nonlinear optical imaging approaches. In general, desires to increase the signal-to-noise ratio through the use of higher peak intensity sources in nonlinear optical imaging are tempered primarily by damage to the samples under such conditions. In cases in which damage is dominated by local heating effects, suppression of fluorescence (from labels or from autofluorescence) could potentially

https://doi.org/10.1021/acs.analchem.3c02638
Anal. Chem. 2023, 95, 14331−14340

provide a sensitive method for directly measuring the localized transient temperature changes induced during beam-scanning imaging. Since this read-out operates in real time with a temporal and spatial resolution set by fluorescence, it is much more direct and quantitative than subsequent visual assessments of gross perturbation to the samples used previously to assess sample damage. Under full-field of view imaging with identical fast-scan conditions, an upper bound on the temperature change per pass through the field of view is given by 1/64th of the temperature induced by 64 serial passes. Under these conditions, the sample temperature is expected to change by ∼0.1 °C during multiphoton excited fluorescence imaging for a single-pass using a fast resonant (8.8 kHz) scan mirror within the central field of view corresponding to ∼0.4 °C/μs. The use of slower galvanometer mirrors has the potential to substantially increase that heating rate. Under identical conditions, a continuous exposure of 100 μs would be expected to produce temperature changes as much as 40 °C. These estimates highlight the importance of fast beam-scanning in minimizing sample damage from local heating in nonlinear optical microscopy in general, and in two-photon excitation for FRWP in particular.

CONCLUSIONS

The development of FRWP with comb pattern photobleaching provides a new analytical tool for fast diffusion events tracking. Compared to point-bleach FRAP, FRWP improves the upper limit of accessible diffusivities, extends the measurement volume to a large FoV, and supports multiphoton excitation with ultrafast fluorescence excitation sources. In this work, FRWP was applied to characterize the mobility of three different biologically relevant macromolecules of varying hydrodynamic radius in aqueous solutions. Effective diffusion coefficients with values up to 200 $\mu m^2/s$ were recovered. Furthermore, it was shown that performing a series of experiments at varying excitation power enables to recover unbiased room-temperature diffusion coefficients by approximating the experimental values to a zero laser power limit. The validity of the recovered diffusivities was confirmed by comparing them with the theoretically predicted values. The observed strong dependence of the apparent mobility of dissolved macromolecules on the incident excitation power was further examined and characterized by simulations accounting for thermal changes in diffusion and photothermal effects. Due to its compatibility with multiphoton excitation, FRWP has the potential to aid in assessing the diffusivity of biomolecules within tissues and other experiments requiring long penetration depths. In sum, FRWP provides a complementary analysis pathway for fast-diffusing biological molecules and expands the application range of non-destructive optical methods for diffusion studies.

ASSOCIATED CONTENT

Supporting Information

The Supporting Information is available free of charge at https://pubs.acs.org/doi/10.1021/acs.analchem.3c02638.

Additional animations to assist in the visualization of FRWP experiments (MOV)

Description of the animations and All MATLAB data analysis algorithms (PDF)

AUTHOR INFORMATION

Corresponding Author

Garth J. Simpson − *Department of Chemistry, Purdue University, West Lafayette, Indiana 47907, United States;* orcid.org/0000-0002-3932-848X; Email: gsimpson@purdue.edu

Authors

Minghe Li − *Department of Chemistry, Purdue University, West Lafayette, Indiana 47907, United States;* orcid.org/0000-0002-6952-3825

Aleksandr Razumtcev − *Department of Chemistry, Purdue University, West Lafayette, Indiana 47907, United States;* orcid.org/0000-0001-9591-8612

Gwendylan A. Turner − *Department of Chemistry, Purdue University, West Lafayette, Indiana 47907, United States*

Yechan Hwang − *Department of Chemistry, Purdue University, West Lafayette, Indiana 47907, United States*

Complete contact information is available at: https://pubs.acs.org/10.1021/acs.analchem.3c02638

Author Contributions

M.L., A.R., G.A.T., and Y.H. performed the experiments, M.L. developed the forward model and performed simulations and data analysis, G.J.S. managed and supervised the project, and all authors contributed to manuscript writing and preparation.

Notes

The authors declare no competing financial interest.

They are publicly available at https://github.itap.purdue.edu/Simpson-Laboratory-for-Nonlinear-Optics/FRWP

ACKNOWLEDGMENTS

The authors gratefully acknowledge funding for the present work from the National Science Foundation (CHE-2004046, CHE-2305178) and from the NSF Center for Bioanalytic Metrology (IIP-1916691).

REFERENCES

(1) Alcor, D.; Gouzer, G.; Triller, A. *Eur. J. Neurosci.* **2009**, *30*, 987−997.

(2) Jin, S.; Haggie, P. M.; Verkman, A. S. *Biophys. J.* **2007**, *93*, 1079−1088.

(3) Veerapathiran, S.; Wohland, T. *Methods* **2018**, *140-141*, 140−150.

(4) Annunziata, O.; Buzatu, D.; Albright, J. G. *Langmuir* **2005**, *21*, 12085−12089.

(5) Patil, S. M.; Keire, D. A.; Chen, K. *AAPS J.* **2017**, *19*, 1760−1766.

(6) Cooper, J. T.; Harris, J. M. *Anal. Chem.* **2014**, *86*, 7618−7626.

(7) Hirvonen, L. M.; Fruhwirth, G. O.; Srikantha, N.; Barber, M. J.; Neffendorf, J. E.; Suhling, K.; Jackson, T. L. *Pharm. Res.* **2016**, *33*, 2025−2032.

(8) Oura, M.; Yamamoto, J.; Ishikawa, H.; Mikuni, S.; Fukushima, R.; Kinjo, M. *Sci. Rep.* **2016**, *6*, 31091.

(9) Lorén, N.; Hagman, J.; Jonasson, J. K.; Deschout, H.; Bernin, D.; Cella-Zanacchi, F.; Diaspro, A.; McNally, J. G.; Ameloot, M.; Smisdom, N.; Nydén, M.; Hermansson, A.-M.; Rudemo, M.; Braeckmans, K. *Q. Rev. Biophys.* **2015**, *48*, 323−387.

(10) Geverts, B.; van Royen, M. E.; Houtsmuller, A. B. Analysis of Biomolecular Dynamics by FRAP and Computer Simulation. *Advanced fluorescence microscopy: Methods and protocols*; Humana: New York, NY 2015, 109−133.

(11) Lippincott-Schwartz, J.; Snapp, E. L.; Phair, R. D. *Biophys. J.* **2018**, *115*, 1146−1155.

(12) Reits, E. A. J.; Neefjes, J. J. *Nat. Cell Biol.* **2001**, *3*, E145.

(13) Dobrucki, J. W.; Feret, D.; Noatynska, A. *Biophys. J.* **2007**, *93*, 1778−1786.
(14) Colin-York, H.; Heddleston, J.; Wait, E.; Karedla, N.; DeSantis, M.; Khuon, S.; Chew, T.; Sbalzarini, I. F.; Fritzsche, M. *Small Methods* **2022**, *6*, No. e2200149.
(15) Xu, F.; Liu, W.; Hanson, M. A.; Stevens, R. C.; Cherezov, V. *Cryst. Growth Des.* **2011**, *11*, 1193−1201.
(16) Thapaliya, E. R.; Zhang, Y.; Raymo, F. M. *J. Mater. Chem. C Mater.* **2017**, *5*, 1179−1183.
(17) Sustr, D.; Hlaváček, A.; Duschl, C.; Volodkin, D. *J. Phys. Chem. B* **2018**, *122*, 1323−1333.
(18) Brown, E. B.; Wu, E. S.; Zipfel, W.; Webb, W. W. *Biophys. J.* **1999**, *77*, 2837−2849.
(19) Dey, D.; Marciano, S.; Nunes-Alves, A.; Kiss, V.; Wade, R. C.; Schreiber, G. *J. Mol. Biol.* **2021**, *433*, No. 166898.
(20) Braeckmans, K.; Peeters, L.; Sanders, N. N.; de Smedt, S. C.; Demeester, J. *Biophys. J.* **2003**, *85*, 2240−2252.
(21) Seiffert, S.; Oppermann, W. *J. Microsc.* **2005**, *220*, 20−30.
(22) Geiger, A. C.; Smith, C. J.; Takanti, N.; Harmon, D. M.; Carlsen, M. S.; Simpson, G. J. *Biophys. J.* **2020**, *119*, 737−748.
(23) Cao, Z.; Harmon, D. M.; Yang, R.; Razumtcev, A.; Li, M.; Carlsen, M. S.; Geiger, A. C.; Zemlyanov, D.; Sherman, A. M.; Takanti, N.; Rong, J.; Hwang, Y.; Taylor, L. S.; Simpson, G. J. *Anal. Chem.* **2023**, *95*, 2192−2202.
(24) Tran-Ba, K.-H.; Higgins, D. A.; Ito, T. *Anal. Chem.* **2015**, *87*, 5802−5809.
(25) Zheng, Q.; Blanchard, S. C. Single Fluorophore Blinking. In *Encyclopedia of Biophysics*; Roberts, G. C. K., Ed.; Springer Berlin Heidelberg: Berlin, Heidelberg, 2013; 2322−2323.
(26) Dempsey, G. T.; Vaughan, J. C.; Chen, K. H.; Bates, M.; Zhuang, X. *Nat. Methods* **2011**, *8*, 1027−1036.
(27) Ross, D.; Gaitan, M.; Locascio, L. E. *Anal. Chem.* **2001**, *73*, 4117−4123.
(28) Jiang, Q.; Rogez, B.; Claude, J.-B.; Baffou, G.; Wenger, J. *ACS Photonics* **2019**, *6*, 1763−1773.
(29) Donner, J. S.; Thompson, S. A.; Kreuzer, M. P.; Baffou, G.; Quidant, R. *Nano Lett.* **2012**, *12*, 2107−2111.
(30) Guo, M.; Xu, Y.; Gruebele, M. *Proc. Natl. Acad. Sci. U. S. A.* **2012**, *109*, 17863−17867.
(31) Dhar, A.; Girdhar, K.; Singh, D.; Gelman, H.; Ebbinghaus, S.; Gruebele, M. *Biophys. J.* **2011**, *101*, 421−430.
(32) Li, M.; Razumtcev, A.; Yang, R.; Liu, Y.; Rong, J.; Geiger, A. C.; Blanchard, R.; Pfluegl, C.; Taylor, L. S.; Simpson, G. J. *J. Am. Chem. Soc.* **2021**, *143*, 10809−10815.
(33) Zhang, Y.; Zong, H.; Zong, C.; Tan, Y.; Zhang, M.; Zhan, Y.; Cheng, J.-X. *J. Am. Chem. Soc.* **2021**, *143*, 11490−11499.
(34) Muir, R. D.; Sullivan, S. Z.; Oglesbee, R. A.; Simpson, G. J. *Rev. Sci. Instrum.* **2014**, *85*, No. 033703.
(35) Jahanban-Esfahlan, A.; Ostadrahimi, A.; Jahanban-Esfahlan, R.; Roufegarinejad, L.; Tabibiazar, M.; Amarowicz, R. *Int. J. Biol. Macromol.* **2019**, *138*, 602−617.
(36) Majorek, K. A.; Porebski, P. J.; Dayal, A.; Zimmerman, M. D.; Jablonska, K.; Stewart, A. J.; Chruszcz, M.; Minor, W. *Mol. Immunol.* **2012**, *52*, 174−182.
(37) Falke, S.; Dierks, K.; Blanchet, C.; Graewert, M.; Cipriani, F.; Meijers, R.; Svergun, D.; Betzel, C. *J. Synchrotron Radiat.* **2018**, *25*, 361−372.
(38) Hink, M. A.; Griep, R. A.; Borst, J. W.; Van Hoek, A.; Eppink, M. H. M.; Schots, A.; Visser, A. J. W. G. *J. Biol. Chem.* **2000**, *275*, 17556−17560.
(39) Langer, A.; Hampel, P. A.; Kaiser, W.; Knezevic, J.; Welte, T.; Villa, V.; Maruyama, M.; Svejda, M.; Jähner, S.; Fischer, F.; Strasser, R.; Rant, U. *Nat. Commun.* **2013**, *4*, 2099.
(40) Gagnon, P.; Nian, R.; Leong, D.; Hoi, A. *J. Chromatogr. A* **2015**, *1395*, 136−142.
(41) Swaminathan, R.; Hoang, C. P.; Verkman, A. S. *Biophys. J.* **1997**, *72*, 1900−1907.
(42) Pucadyil, T. J.; Chattopadhyay, A. *J. Fluoresc.* **2006**, *16*, 87−94.
(43) Hortin, G. L.; Sviridov, D.; Anderson, N. L. *Clin. Chem.* **2008**, *54*, 1608−1616.
(44) Wang, W.; Wang, E. Q.; Balthasar, J. P. *Clin. Pharmacol. Ther.* **2008**, *84*, 548−558.
(45) Armstrong, J. K.; Wenby, R. B.; Meiselman, H. J.; Fisher, T. C. *Biophys. J.* **2004**, *87*, 4259−4270.
(46) Wang, D.; Liu, J.; Liu, Z.; Zhang, Z.; Sun, Z.; Wu, C.; Wang, G. *ACS Appl. Nano Mater.* **2020**, *3*, 2214−2220.
(47) Blumm, J.; Lindemann, A. *High Temp. High Press.* **2003**, *35/36*, 627−632.
(48) Tiede, L. M.; Nichols, M. G. *Photochem. Photobiol.* **2006**, *82*, 656−664.
(49) Galli, R.; Uckermann, O.; Andresen, E. F.; Geiger, K. D.; Koch, E.; Schackert, G.; Steiner, G.; Kirsch, M. *PLoS One* **2014**, *9*, No. e110295.
(50) Hopt, A.; Neher, E. *Biophys. J.* **2001**, *80*, 2029−2036.

https://doi.org/10.1021/acs.analchem.3c02638
Anal. Chem. 2023, 95, 14331−14340